

Elastic strain relaxation in discontinuous wetting layers and its impact on lateral ordering of heteroepitaxial dots

M. Hanke,¹ T. Boeck,² A.-K. Gerlitzke,² F. Syrowatka,³ and F. Heyroth³

¹Martin-Luther-Universität Halle-Wittenberg, Fachbereich Physik, Hoher Weg 8, D-06120 Halle/Saale, Germany

²Institut für Kristallzüchtung, Max-Born-Straße 2, D-12489 Berlin, Germany

³Interdisziplinäres Zentrum für Materialwissenschaften, Hoher Weg 8, D-06120 Halle/Saale, Germany

(Received 30 August 2006; published 10 October 2006)

We discuss morphological changes of strained SiGe/Si(001) dots grown from an indium solution. In the course of a particular depletion scenario initial, lenslike dots transform into truncated pyramids of fourfold symmetry inside circular rims of rising height and steep inner edge. Further dot nucleation performs close to the rim indicating elastically relaxed lattice sites. The observations made are supported by numerical finite element calculations on the strain energy distribution.

DOI: [10.1103/PhysRevB.74.153304](https://doi.org/10.1103/PhysRevB.74.153304)

PACS number(s): 68.65.-k, 68.37.Hk, 81.15.Lm

Condensed matter at zero dimensionality has promoted an overwhelming research effort comprising a zoo of fabrication techniques and analytical tools.¹⁻⁴ In many cases self-formation of semiconductor dots^{5,6} can provide a suitable alternative to expensive and time-consuming template based approaches.⁷ Within the Stranski-Krastanow process a heteroepitaxial layer initially wets the surface and the strain energy increases with thickness. Beyond a critical value planar wetting becomes, however, unstable in favor of three-dimensional growth as the energy gain due to elastic relief overcompensates additional free surface.⁸ Since molecular beam epitaxy (MBE) approaches a more kinetically restricted regime, dot nucleation from a metallic solution during liquid phase epitaxy (LPE), cooling rates of less than 0.2 K/min provided, enables growth studies extremely close to thermodynamic equilibrium. Shape transformation⁹⁻¹³ and assembling phenomena¹⁴⁻¹⁹ of heteroepitaxial dots are frequently discussed within these limits, whereas SiGe on silicon has widely served as a model system. One of the most obvious, however, hardly recognized differences manifest in the dot orientation. Since MBE based SiGe/Si(001) dots form {10} side facets,^{20,21} respective LPE dots depict {11} facets.^{22,23} Elastic strain, caused by buried dots and mediated by subsequent spacer layers, supports vertical positional replication^{14,15} and may also improve lateral assembling within subsequent layers of dot stacks.¹⁹ Strain propagation within a single heteroepitaxial layer, on the other hand, remains a surface-mediated process, which strongly relates dot assembling to the particular relaxation behavior within the wetting layer.

Here we discuss the formation of a discontinuous, nonuniform wetting layer and its implications for the lateral self-formation of heteroepitaxial dots. Samples have been grown by means of LPE applying a slide-boat setup. There a target substrate is placed underneath a horizontally movable graphite frame which contains the liquid solution. In a first step the indium solution has been fully saturated with silicon at 930 °C whereas the amount of germanium (3.551 g) added to 50-g indium corresponds to 10% germanium in the solid state. In order to ensure a clean growth environment the entire LPE process performs under a pure hydrogen flux. After a mandatory annealing step at 930 °C for 1 h to remove the

natural oxide layer and a homogenization of the solution for 3 h, the frame is placed on top of the Si(001) substrate. Then a constant gradient of 0.16 K/min is applied during an overall temperature ramp from 930 to 920 °C, which initiates the heteroepitaxial growth. However, to get an *ex situ* access to initial and intermediate growth stages the frame (containing the liquid solution) was moved forward by approximately 3 mm after 6, 9, and 12 min. Thus adjacent sample positions provide stages according to temperature ramps ΔT of 1, 1.5, 2, and 10 K which enables a detailed reconstruction of the growth scenario later on. Therefore we have applied a field emission scanning electron microscope (Philips XL30) operated at primary electron energies of 2 and 12 kV for top view and side view images, respectively.

Incipient heteroepitaxial stages have been revealed by stripping the solution after an applied ramp from 930 to 929 °C. Tiny surface undulations, Fig. 1(a), provide elastic relief at the expense of additional free surface. It is noteworthy that the developing pattern tends to step bunching whereas the step density subsequently increases on the slopes. Eventually the wetting layer shrinks between initial stages resulting in lenslike SiGe dots with an average height of 410 nm along a base diameter of 1.7 μm , Fig. 1(b). The inset displays an intermediate quadruplet with preferential $\langle 100 \rangle$ orientation. Lateral assembling, mediated by prior surface undulations, inherently happens before the final dot shape evolves. The nucleation of dots with increased lattice mismatch, on the other hand, performs on a much faster time scale than the evolution of lateral ordering.^{16,17}

During the following growth sequence the temperature was lowered to 928.5 °C. Circular dots split into a central truncated pyramid (d1) with {111} side facets and an asymmetrically shaped rim (w) enclosing uncovered silicon substrate (sub), Fig. 1(c). This process is obviously supported by further strain relaxation at the free-standing side facets. Typical widths and heights of walls surrounding individual dots are 270 nm and about 45 nm, respectively. Even more extended rings, inset of Fig. 1(c), have been observed, e.g., around quadruplets of fully developed dots. LPE relies on a finite material reservoir, so that the liquid solution becomes undersaturated in the course of dot nucleation. Strain induced material transport from the wetting layer as well as from the

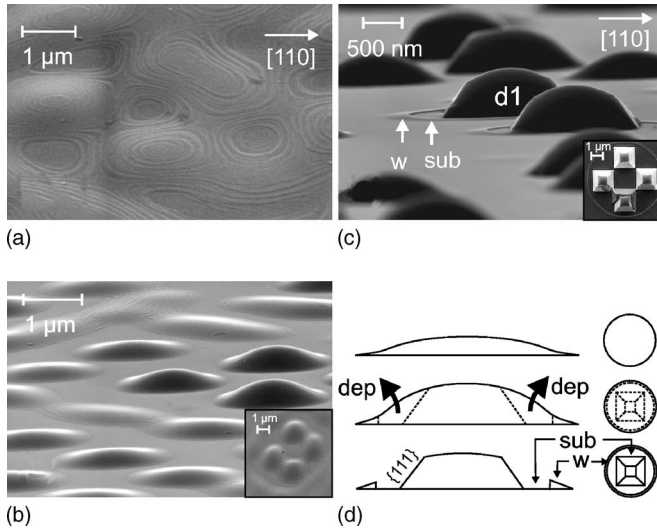


FIG. 1. The initial growth sequence starts with surface undulations which are formed by discrete vertical steps (a). Individual lenslike dots subsequently appear (b) with preferential $\langle 100 \rangle$ direction (inset therein). They transform during later stages (c) into truncated pyramids (d1) with four adjacent $\{111\}$ side and a single $\{001\}$ top facet. Strain induced depletion (dep) yields uncovered silicon substrate (sub) and asymmetrically shaped walls (w) surrounding single dots and dot ensembles (inset). (d) depicts the subsequent stages (a) through (c) in side and top view.

dots back into the liquid solution becomes very likely since the nucleation performs close to equilibrium. Figure 1(d) illustrates the observed depletion (dep) which transfers round-shaped dots into fourfold pyramids surrounded by asymmetrically shaped rims. Moreover, the fourfold symmetry of the depletion inside the rim indicates a strain mediated shape transformation. Trench formation near MBE grown SiGe dots²⁴ is also strain mediated. However, the material moves from the substrate into the dot.

Due to the subsequently performed cooling to 928 °C the solution becomes oversaturated which causes further nucleation. Small dots (d2) in Fig. 2(b) indicate favorable nucleation sites along $\langle 100 \rangle$ near the rim. However, their distribution eventually becomes quite uniform, Fig. 2(a). Obviously the discontinuity at the rim provides elastic relief due to the lack of lateral mechanical confinement.

Nucleation at the rim and the observed occupation sequence can be explained by numerical finite element calculations on the strain energy density $(E/V)_{strain}$, which is given by $2c_{44}(c_{11}+2c_{12})/c_{11}[(\epsilon_{xx}^2+\epsilon_{yy}^2+\epsilon_{zz}^2)+1/2(\epsilon_{xy}^2+\epsilon_{xz}^2+\epsilon_{yz}^2)]$. c_{ij} and ϵ_{ij} are the elastic constants within a cubic system and calculated strain components, respectively. Note that only a quarter of the actual models in Figs. 3(a) and 3(b) is considered due to quasiperiodic boundary conditions applied to the outer edges. Both calculations consider a germanium content of 10% within the wetting layer and the dot, which refers to a lattice mismatch of 0.42%. A truncated pyramid with $\{111\}$ side and a single $\{001\}$ top facet placed on a planar wetting layer of 30 nm, Fig. 3(a), results in a strain energy density, Fig. 3(c), which basically expresses Young's modulus.^{17,24} Figure 3(b) shows, on the other hand, a more lifelike model similar to the experimentally observed

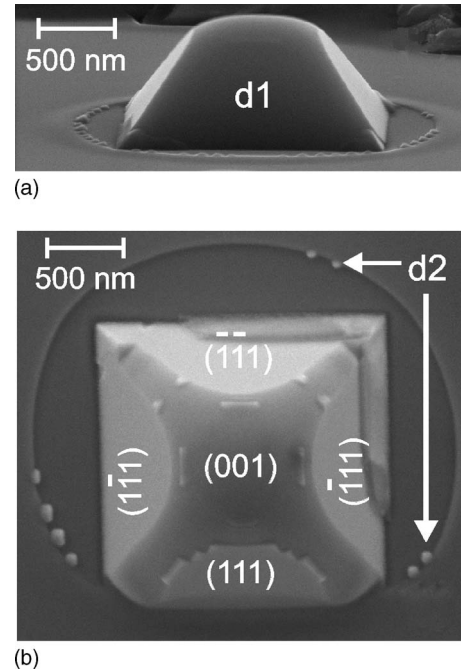


FIG. 2. Inclined (a) and top view scanning electron micrographs (b) of individual dots (d1) surrounded by circular walls which are decorated with considerably smaller dots (d2).

in Fig. 1(c). It considers a depleted area surrounded by an asymmetrically shaped wall. A nonuniform wetting layer tremendously alters the elastic behavior. Figure 3(d) indicates an elastically relaxed wall due to the discontinuity, however, diverse energy minima develop. Related areas inside the depleted region, denoted $M_{[110]}$ and $M_{\bar{1}\bar{1}0}$, approach the silicon lattice, hence they are not suitable candidates for an ongoing nucleation. However, another type of minima appears within the rim itself, $M_{[100]}$, which indicates initial decoration along the $\langle 100 \rangle$ direction.

The nucleation scenario around a single dot, comprising wetting layer depletion and subsequent dot decoration at the rim, applies for dot dimers and longer formations as well. Figure 4(a) displays chains of dots still joining the rim around an initial dimer. The main orientation of the rim along the mechanically softer $\langle 100 \rangle$ directions refers to the dimer axis, which itself results from the orientation of the prior surface undulations as shown in Fig. 1(a). Thus as soon as the fourfold symmetry of a separated single dot (d1), Fig. 2, is reduced to a twofold symmetry of a linear dimer (d1-d1), Fig. 4(a), succeeding dots (d2) are subject to linear self-assembling into chains along the $\langle 100 \rangle$ direction. After an overall growth time of 60 min, corresponding to a temperature gradient of 10 K the dot size and the average distance between them increase and eventually leads to dots (d3) which are distinctly apart from the wetting layer, Fig. 4(b).

Both types, initial (d1) and succeeding dots (d2) have been formed due to elastic strain relaxation. However, diverse morphologies suppose different growth conditions. An undersaturated indium solution, caused by the extensive incorporation of silicon within the initial $\text{Si}_{0.9}\text{Ge}_{0.1}$ dots and the strain-induced partial depletion of the wetting layer, implies different thermodynamic conditions for both. This will affect

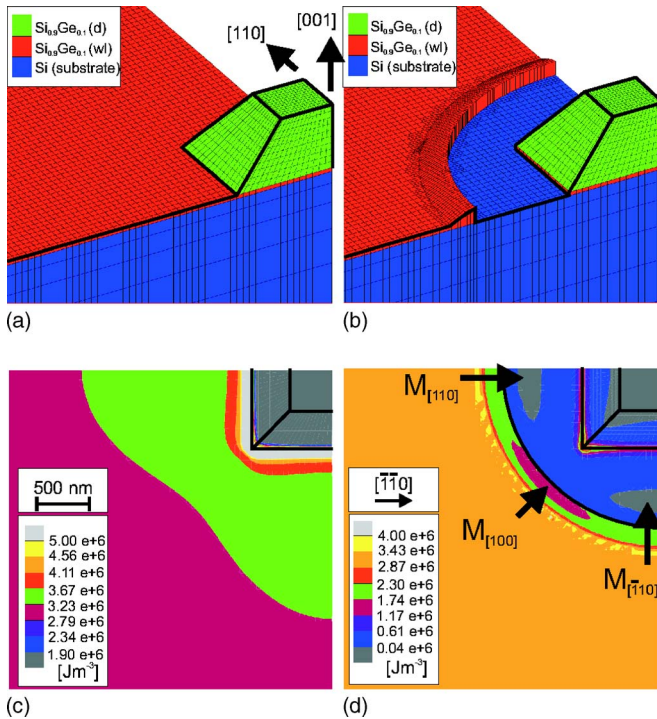


FIG. 3. (Color online) The strain energy distribution around a single $\text{Si}_{0.9}\text{Ge}_{0.1}/\text{Si}(001)$ dot on a continuous and planar wetting layer (a) results in the well-known (Ref. 24) distribution (c) where the lattice relaxes more sufficient along the elastically softer $\langle 100 \rangle$ direction. However, a wetting layer which is partially depleted and confined by an asymmetrically shaped wall (b), as experimentally observed in Fig. 1(c), yields an *absolute* energy minimum $M_{[100]}$ along $\langle 100 \rangle$. The other indicated minima $M_{[110]}$ and $M_{[\bar{1}\bar{1}0]}$ figure in the depleted area.

the incorporation of germanium and hence the dot size. Energy dispersive x-ray (EDX) microanalysis yields a measure of the averaged dot composition and vice versa probes the local growth conditions. The applied EDX parameters ensure an effective suppression of the underlying silicon substrate due to a neglectable penetration depth. Electrons with a comparatively low primary energy of 5 keV illuminate the sample under a very glancing angle of 5° and hence restrict the probed volume mainly to the dots themselves. Nevertheless the EDX values account for a lower limit of the germanium content in the dot. Figure 5 shows three spectra taken out of depleted areas of the silicon substrate (sub), out of a single parental dot (d1) and from a single dot at the rim (d3). Evaluating the intensity ratios of the Si-K and Ge-L edges results in germanium contents of $c_{\text{sub}} < 1\%$, $c_{d1} = 8.3\%$, and $c_{d3} = 19.6\%$, respectively. Since c_{d1} corresponds well with the aspired content of 10%, the smaller dots incorporate more than twice the relative amount. Strain-induced resolving of wetting layer material obviously enables further dot growth, however, the operating point in the phase diagram has been shifted towards higher germanium contents.

In conclusion, we have discussed strain-mediated morphological changes during heteroepitaxial growth of $\text{SiGe}/\text{Si}(001)$ dots. Further on the impact of a nonuniform, discontinuous wetting layer on the lateral assembling of heteroepitaxial dots has been studied. The experimental results

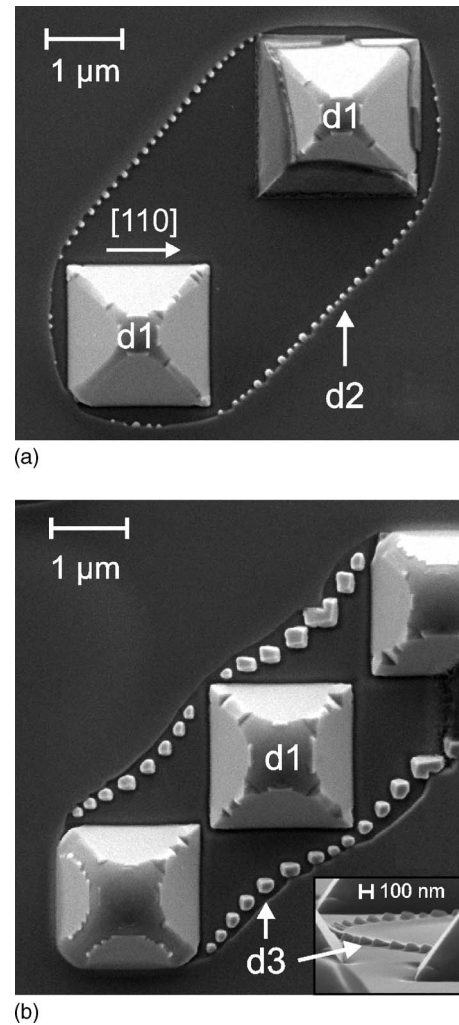


FIG. 4. A partially straight wall (a) around dimers (d1-d1) yields linearly self-assembled dots (d2). Further growth results in detached dots (d3) along the inner rim path (b) whereas the dot size increases with respect to those which are still connected to the wetting layer. The inset (b) proves a vertical extent beyond the average wetting layer plateau.

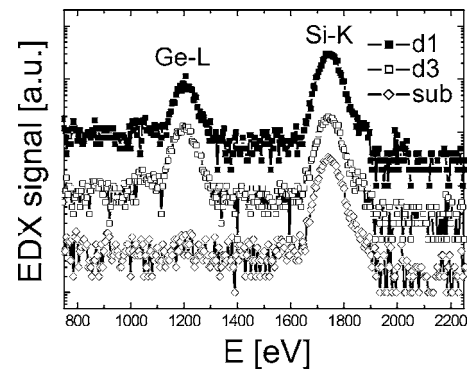


FIG. 5. Energy dispersive x-ray spectroscopy yields approximately $\text{Si}_{0.917}\text{Ge}_{0.083}$ within the initial dots (d1), a considerably higher germanium content of approximately 19.6% within the subsequently formed, separated dots (d3) and nearly pure silicon ($>99\%$) at depleted areas. Curves are vertically shifted for better view.

from low misfit liquid phase epitaxy are supported by numerical finite element calculations on the strain energy density. Initial elastic strain relief induces surface undulations, which transform into lenslike SiGe dots. The subsequent transition into faceted dots of fourfold symmetry is accompanied by a partial wetting layer depletion forming asymmetrically shaped, circular rims of rising height and a steep inner edge. In general, areas close to the rim provide an elastically relaxed lattice due to the lack of lateral mechanical confinement, which is confirmed by further dot decora-

tion and finite element calculations. Our calculations imply different relaxation behaviors on uniform and discontinuous wetting layers.

M.H. acknowledges funding by the Federal State of Sachsen-Anhalt, Germany, within the Cluster of Excellence (CoE) *Nanostructured Materials*, project NW3 and the German Research Foundation, Grant No. HA3495/3. We thank Rolf Köhler, Humboldt-University, Berlin, for continuous support and interest.

-
- ¹V. A. Shchukin, N. N. Ledentsov, and D. Bimberg, *Epitaxy of Nanostructures* (Springer, New York, 2004).
- ²M. A. Herman, W. Richter, and H. Sitter, *Epitaxy, Physical Principles and Technical Implementations* (Springer, Berlin, 2004).
- ³J. Stangl, V. Holý, and G. Bauer, *Rev. Mod. Phys.* **76**, 725 (2004).
- ⁴M. S. Skolnick and D. J. Mowbray, *Annu. Rev. Mater. Sci.* **34**, 181 (2004).
- ⁵D. J. Eaglesham and M. Cerullo, *Phys. Rev. Lett.* **64**, 1943 (1990).
- ⁶Y.-W. Mo, D. E. Savage, B. S. Swartzentruber, and M. G. Lagally, *Phys. Rev. Lett.* **65**, 1020 (1990).
- ⁷S. Kiravittaya, A. Rastelli, and O. G. Schmidt, *Appl. Phys. Lett.* **88**, 043112 (2006).
- ⁸D. J. Srolovitz, *Acta Metall.* **37**, 621 (1989).
- ⁹M. Hanke, M. Schmidbauer, D. Grigoriev, H. Raidt, P. Schäfer, R. Köhler, A.-K. Gerlitzke, and H. Wawra, *Phys. Rev. B* **69**, 075317 (2004).
- ¹⁰P. Sutter, P. Zahl, and P. Sutter, *Appl. Phys. Lett.* **82**, 2003 (2003).
- ¹¹M. Meixner, E. Schöll, V. A. Shchukin, and D. Bimberg, *Phys. Rev. Lett.* **87**, 236101 (2001a).
- ¹²E. Sutter, P. Sutter, and J. E. Bernard, *Appl. Phys. Lett.* **84**, 2262 (2004).
- ¹³M. Hanke, T. Boeck, A.-K. Gerlitzke, F. Syrowatka, F. Heyroth, and R. Köhler, *Appl. Phys. Lett.* **86**, 142101 (2005).
- ¹⁴J. Tersoff, C. Teichert, and M. G. Lagally, *Phys. Rev. Lett.* **76**, 1675 (1996).
- ¹⁵G. Springholz, V. Holý, M. Pinczolit, and G. Bauer, *Science* **282**, 734 (1998).
- ¹⁶M. Meixner, E. Schöll, M. Schmidbauer, H. Raidt, and R. Köhler, *Phys. Rev. B* **64**, 245307 (2001).
- ¹⁷M. Hanke, H. Raidt, R. Köhler, and H. Wawra, *Appl. Phys. Lett.* **83**, 4927 (2003).
- ¹⁸M. Hanke, T. Boeck, A.-K. Gerlitzke, F. Syrowatka, and F. Heyroth, *Appl. Phys. Lett.* **88**, 063119 (2006).
- ¹⁹M. Schmidbauer, S. Seydmohamadi, D. Grigoriev, Z. M. Wang, Y. I. Mazur, P. Schäfer, M. Hanke, R. Köhler, and G. J. Salamo, *Phys. Rev. Lett.* **96**, 066108 (2006).
- ²⁰J. Tersoff, B. J. Spencer, A. Rastelli, and H. von Känel, *Phys. Rev. Lett.* **89**, 196104 (2002).
- ²¹A. Rastelli, M. Stoffel, J. Tersoff, G. S. Kar, and O. G. Schmidt, *Phys. Rev. Lett.* **95**, 026103 (2005).
- ²²P. O. Hansson, M. Albrecht, W. Dorsch, H. P. Strunk, and E. Bauser, *Phys. Rev. Lett.* **73**, 444 (1994).
- ²³W. Dorsch, H. P. Strunk, H. Wawra, G. Wagner, J. Groenen, and R. Carles, *Appl. Phys. Lett.* **72**, 179 (1998).
- ²⁴U. Denker, O. G. Schmidt, N. Y. Jin-Phillip, and K. Eberl, *Appl. Phys. Lett.* **78**, 3723 (2001).